Shock Waves (2006) 15:363–373
DOI 10.1007/s00193-006-0018-1

ORIGINAL ARTICLE

Shock-induced near-wall two-phase flow structure over a micron-sized particles bed

B. Y. Wang · Y. Xiong · L. X. Qi

Received 16 September 2003 / Accepted 6 May 2004 / Published online: 14 June 2006

Abstract The present paper studies numerical modelling of near-wall two-phase flows induced by a normal shock wave moving at a constant speed, over a micron-sized particles bed. In this two-fluid model, the possibility of particle trajectory intersection is considered and a full Lagrangian formulation of the dispersed phase is introduced. The finiteness of the Reynolds and Mach numbers of the flow around a particle as well as the fineness of the particle sizes are taken into account in describing the interactions between the carrier- and dispersed-phases. For the small mass-loading ratio case, the numerical simulation of flow structure of the two phases is implemented and the profiles of the particle number density are obtained under the constant-flux condition on the wall. The effects of the shock Mach number and the particle size and material density on particle entrainment motion are discussed in detail. The obtained results indicate that interphase non-equilibrium in the velocity and temperature is a common feature for this type of flows and a local particle accumulation zone may form near the envelope of the particle trajectory family.

Keywords Moving shock wave · Particle entrainment · Two-phase flow · Numerical modelling

PACS 47.40.-x · 47.55.Kf · 47.15.Cb

Communicated by Z. Jiang.

B. Y. Wang (✉)· Y. Xiong · L. X. Qi
LNM, Institute of Mechanics,
Chinese Academy of Sciences,
Beijing 100080, China
e-mail: wby@imech.ac.cn

1 Introduction

A two-phase flow may be induced when a shock wave travels over an erodible particles bed. The knowledge of mechanism and effects of particle entrainment from the bed surface into the air is of fundamental importance for preventing fires and explosions in various powder processing facilities and coal mines or in workrooms and plants with deposited particles on the ground. Compared to gaseous mixtures, reactive gas–particle suspensions have extremely high rich explosion limits [1]. Particularly, in some industrial production occasions, dust explosions starting from a flame generated by an ignition source can be transmitted through pneumatic transport systems to different parts of a processing facility and this may cause a large amount of damage. Moreover, dust mixtures can sustain a deflagration that may lead to a self-sustained detonation wave in tubes of sufficient diameter and length [2]. The mechanism of detonation propagation in such systems is not fully understood. For instance, the work by Khasainov and Veyssiere [3] and Veyssiere et al. [4] revealed the existence of three different detonation modes in some particle concentration ranges: single-front detonation (SFD), pseudo-gas detonation (PGD) and double-front detonation (DFD). The possibility of multiple detonation regimes and other novel characteristics relevant to the two-phase mixtures lead to more interests in experimental and numerical investigations of heterogeneous detonation [5–8]. Generally, a particles suspension must be present before a dust explosion can occur. However, for many real situations in engineering process or in nature, dust suspensions do not exist originally but form by an earlier and smaller explosion (primary explosion). In other words, when a shock wave, which may originate from a

gaseous explosive source, propagates over a surface laden with particles, these particles may be raised owing to the lift force resulting from the local flow shear of the shock-induced gas boundary layer. As a result, behind the shock front, a gas–particle suspension (known as a dust cloud) appears and then the dispersed particles may be ignited by the explosion flames already present. In this way, a primary gaseous explosion can develop into a secondary dust explosion. In the assessment of dust explosion hazard, various critical parameters (maximum pressure, rate of pressure rise, time delay, detonation velocity and so on) depend on the dust concentration and particle size. Of course, the dust concentration must lie within the lower and upper explosibility limits if the flame is to propagate through a dust cloud and there is a general tendency for the explosibility of dusts to increase as the particle size decreases. In addition, researches on the interaction between a detonation wave and a suspension or a layer of combustible particles may also be useful for improving detonation-based propulsion systems such as the ram accelerators. In this connection, the present paper attempts to study the formation and structure of a dust cloud behind a normal shock wave moving at a constant speed along a flat wall deposited with micron-sized particles.

In our model, the shear lift force induced by the gas boundary layer flow is considered as the unique mechanism of particle rising from the deposit surface. During recent decades, effects of the lift force on shock-induced near-wall flows of the gas–particle mixture is a continuing study area in the literature [9–13]. Because of the action of the lift force as well as the gravity, trajectories of the entrained particles intersect inside the dust cloud. Obviously, it leads to multiple values of the particle flow parameters and makes the problem of calculating the flow structure much more complicated. Therefore, for most numerical works mentioned above, individual particle trajectories and then the cloud height were calculated but the dust flow field was not obtained. Thevand and Daniel [13] gave the particle density and velocity distributions by an Eulerian approach but their method is applicable only in the flow region where the particle trajectories do not intersect each other. To overcome the difficulty caused by non-uniqueness of the particle flow field, we adopt a full Lagrangian approach and develop a numerical scheme to calculate the dispersed-phase parameters along fixed particle trajectories. In particular, we solve the particle continuity equation in the Lagrangian form instead of that in the Eulerian one. This method demands much less computation time than ordinary Lagrangian methods for the dispersed phase. Besides, in our model, the finiteness of the Reynolds and Mach numbers as well as the fineness of the particle sizes are taken into account since the motion of micron-sized particles in a shock-induced gas boundary layer is under consideration.

In shock-fixed coordinates, we present general formulation and similarity criteria for the near-wall two-phase flows with zones of intersecting particle trajectories. The velocity, temperature and particle number-density profiles are obtained over a wide range of control parameters where the particle loadings are kept at small values. In the present work, we pay particular attention to the particle entrainment motion and employ, when performing numerical simulations, the so-called one-way coupling approach [14,15]. With the one-way model, the gas flow is independently solved and the particle motion is determined by the flow field of the carrier phase. In the small mass-loading-ratio case, it is possible to neglect the effect of the particles on the carrier-phase flow. In fact, this is a real situation for the near-wall two-phase flows induced by the laminar gas boundary layer behind a moving shock wave over a micro-sized particles bed under consideration. Generally speaking, the two-way model (i.e. allowance for the influence of the particle presence) is not a fundamental complication in numerical modelling but the one-way model leads to simplification in numerical solution and clearness in mechanism explanation.

2 Numerical modelling

For a gas boundary layer induced by a normal shock wave moving along a flat surface, the flow is laminar at its initial stage adjacent to the shock front. When the shock wave travels at a constant speed U^* (or Mach number M), it is convenient to introduce the Cartesian coordinate system (x^*, y^*) fixed to the shock front (here the x^*- and y^*- axes are along the wall and the front, respectively). Hence, a non-stationary flow of the gas–particle mixture in the laboratory reference framework reduces to a steady-state motion over a wall, which moves at the same value of the wave speed U^* but in the opposite direction. In this work, the wall temperature T_{w}^* is considered a constant and the gas ahead of the shock front keeps the same temperature as that of the wall. In addition, in the gas boundary layer, the temperature dependence of the viscosity μ^* and thermal conductivity k^* of the carrier phase can be assumed to be linear: $\mu^*/\mu_0^* = k^*/k_0^* = KT^*/T_0^*$ (here K is a constant). In the present paper, the superscript $*$ refers to the dimensional quantities when necessary and the subscript 0 to the gas flow parameters in the inviscid region just behind the shock front.

In general, the gas–particle mixture resulting from the shock-induced flow over a particles bed is a dilute two-phase system. Similar to Marble [16], the assumptions adopted in our two-fluid model are as follows. (1) The carrier phase is a perfect compressible gas with constant ratio of specific heats γ. (2) The dispersed phase consists of solid spheres of the same radius σ^* and mass m^*. The material density of the particles $\rho_s^0 = 3m^*/4\pi\sigma^{*3}$ is much larger than that of the gas and then the inertia effect of the particles is taken into account. (3) The volume fraction of the particles and mutual collisions among the particles are negligible and then the dispersed phase is a zero-self-stress fluid. (4) For the solid particles of micron sizes, Brownian motion is ignored but the Knudsen effect is considered for the flow around a particle. (5) No chemical reactions and phase changes are involved in the two-phase system under consideration. (6) The force and heat transfer exerted on the dispersed phase by the carrier phase is the sum of the forces and heat fluxes on a single sphere in a viscous fluid. (7) In the shock-induced flow case, the finiteness effects of the Reynolds and Mach numbers of the flow around a particle are considered. (8) Except for the aerodynamic drag and lift forces caused by the gas boundary layer, the gravity effect on the particle motion is included.

For the problem considered, the aerodynamic entrainment mechanism leads to saltation-like motion of the particles and intersection of particle trajectories. However, it should be pointed out that this does not mean failure of the dilute dust-suspension model. As well known, the average distance between the particles in a dilute gas–particle system is large compared with their linear dimensions, and this criterion is generally satisfied when loadings of the particles are low. Thus it is easy to understand that inside the entrained dust cloud, the mixture may maintain the characteristics of a dilute suspension as only two or three particle trajectories traverse the same field point and then particle loading ratios remain to be the same order of magnitude in the flow field. In other words, the volume fraction of the particles can be neglected even in those zones of intersecting particle trajectories. In addition, based on two-phase fluid dynamics, any space point in the flow field is actually an infinitely small volume element, which contains a very great number of gas molecules and solid particles. Within the framework of the dilute model, there exist a lot of particles but no mutual collisions among the particles in every volume element. In this sense, the particles which move, respectively, along two trajectories, intersecting at a field point, interpenetrate each other and do not come into collision when they cross the relevant volume element. Therefore, the particle motion is still controlled by local aerodynamic forces but not by particle–particle collisions.

Based on the previous works of Carlson and Hoglund [17], Fuchs [18], Saffman [19] and Mei [20], the force and heat transfer on a single spherical particle can be expressed as (the subscript s refers to the solid particles):

$$\mathbf{f}_s^* = m^*\mathbf{g}^* + 6\pi\sigma^*\mu^*(\mathbf{V}^* - \mathbf{V}_s^*)D \\ -6.46\sigma^{*2}\left(\rho^*\mu^*\left|\partial u^*/\partial y^*\right|\right)^{1/2}H(u^* - u_s^*)\mathbf{j}, \quad (1)$$

$$q_s^* = 4\pi\sigma^* k^*(T^* - T_s^*)G. \quad (2)$$

Here $\mathbf{V}^*$, T^* and ρ^* are the velocity vector (its components in x^*- and y^*-axes are u^* and v^*, respectively), temperature and density, respectively; $\mathbf{j}$ the unit vector along the y^*-axis; $\mathbf{g}^*$ the acceleration due to gravity. In order to take into account the finiteness of the Reynolds and Mach numbers and the fineness of the particle sizes, three correction functions D, H and G are introduced as follows. For the aerodynamic drag:

$$D = (1 + Re_s^{2/3}/6)\Phi, \\ \Phi = \left(1 + \exp(-0.427M_s^{-4.63} - 3Re_s^{-0.88})\right)/\phi, \quad (3) \\ \phi = 1 + Kn_s\left(2.57 + 0.68\exp(-1.86/Kn_s)\right).$$

For the shear lift force:

$$H = 0.469\left(1 - \exp(-0.1Re_s)\right)(Re_g/Re_s)^{1/2} \\ + \exp(-0.1Re_s), \quad \text{for} \quad Re_s \le 40; \quad (4) \\ H = 0.0741Re_g{}^{1/2}, \quad \text{for} \quad Re_s > 40.$$

For the heat transfer:

$$G = \left(1 + 0.3Pr^{1/3}Re_s^{1/2}\right)/\Psi, \quad (5) \\ \Psi = 1 + 2.30Kn_s\left(1 + 0.3Pr^{1/3}Re_s^{1/2}\right)/Pr.$$

In these expressions (3)–(5), $Re_s = 2\sigma^*\rho^*\left|\mathbf{V}^* - \mathbf{V}_s^*\right|/\mu^*$ is the slip Reynolds number; $Re_g = \sigma^{*2}\rho^*\left|\partial u^*/\partial y^*\right|/\mu^*$ the shear Reynolds number; $M_s = \left|\mathbf{V}^* - \mathbf{V}_s^*\right|/c^*$ the slip Mach number (here c^* is the gas speed of sound); $Kn_s = 1.255\sqrt{\gamma}M_s/Re_s$ the particle Knudsen number; $Pr = c_p^*\mu^*/k^*$ the gas Prandtl number (here c_p^* is the specific heat at constant pressure).

As mentioned above, owing to the action of the lift and gravity forces, some zones with intersecting particle trajectories may appear inside the dust cloud and the possible intersections of particle trajectories should be taken into account in calculating the near-wall two-phase flow structure. For this purpose, governing equations of the dispersed phase are written for a particle continuum (denoted by the subscript i) along its trajectory and is the so-called full Lagrangian approach. At any point in the flow field, for the velocity and

temperature of the particles there are as many values as there are intersecting trajectories while for the number density of the particles a unique value is equal to the sum of all continua traversing across that point. Although governing equations of the carrier phase are written in the usual Eulerian form, at the point of space under consideration, the source terms concerning interphase coupling must include all the interactions caused by each individual particle continuum traversing across that point.

For generality, in the formulation of the shock-induced near-wall two-phase flows, the following dimensionless variables are introduced:

$$x = \frac{x^*}{l^*}, \quad \eta = \frac{y^*}{l^*}Re^{1/2}, \quad u = \frac{u^*}{U_0^*}, \quad v = \frac{v^*}{U_0^*}Re^{1/2},$$
$$T = \frac{T^*(U^* - U_0^*) + U_0^* T_{\mathrm{w}}^* - U^* T_0^*}{(T_{\mathrm{w}}^* - T_0^*)U_0^*},$$
$$\rho = \frac{\rho^*}{\rho_0^*}, \quad n_{\mathrm{s}} = \frac{n_{\mathrm{s}}^*}{n_{\mathrm{s}}^0}Re^{-1/2}, \quad p = \frac{p^*}{\rho_0^* U_0^{*2}}, \quad \mu = \frac{\mu^*}{\mu_0^*},$$

where p and n_{s} are the gas pressure and particle number density, respectively. In addition, the length scale $l^* = m^* U_0^*/6\pi\sigma^*\mu_0^*$ is taken equal to the phase velocity relaxation length for Stokes drag [16] and the flow Reynolds number $Re = \rho_0^* U_0^* l^*/\mu_0^*$ is based on the characteristic length l^*. Then, for the carrier phase, similar to the laminar boundary layer flows of a pure gas over a semi-infinite flat plate, the following dimensionless governing equations are written in the stretched coordinates (x, η):

$$\frac{\partial \rho u}{\partial x} + \frac{\partial \rho v}{\partial \eta} = 0,$$
$$\rho\left(u\frac{\partial u}{\partial x} + v\frac{\partial u}{\partial \eta}\right) = K\frac{\partial}{\partial \eta}\left(\theta\frac{\partial u}{\partial \eta}\right) - \frac{\partial p}{\partial x} - \alpha K\theta\sum_i n_{\mathrm{s}i}(u - u_{\mathrm{s}i})D_i,$$
$$\rho\left(u\frac{\partial T}{\partial x} + v\frac{\partial T}{\partial \eta}\right) = \frac{K}{Pr}\frac{\partial}{\partial \eta}\left(\theta\frac{\partial T}{\partial \eta}\right) + (a-1)Ec\left[K\theta\left(\frac{\partial u}{\partial \eta}\right)^2 + u\frac{\partial p}{\partial x} + \alpha K\theta\sum_i n_{\mathrm{s}i}(u - u_{\mathrm{s}i})^2 D_i\right] - \frac{2\alpha}{3Pr}K\theta\sum_i n_{\mathrm{s}i}(T - T_{\mathrm{s}i})G_i,$$
$$\frac{\partial p}{\partial \eta} = 0,$$
$$\rho\theta = \frac{2\gamma + \gamma(\gamma-1)M^2}{2\gamma M^2 - (\gamma - 1)}p, \tag{6}$$

with

$$\theta = \frac{T^*}{T_0^*} = \frac{(d-1)T + a - d}{a - 1}. \tag{7}$$

It is known that, in a boundary layer on a flat plate at zero incidence, the gas pressure keeps unchanged: $p = p_{\mathrm{e}} = p_0 = \mathrm{const}$ (here the subscript e refers to the outer flow parameters). Therefore, the derivative term $\partial p/\partial x$ can be omitted and the state equation reduces to $\rho\theta = 1$. In Eq. (6), four dimensionless parameters are defined as

$$a = \frac{U^*}{U_0^*}, \quad d = \frac{T_{\mathrm{w}}^*}{T_0^*}, \quad Ec = \frac{U_0^{*2}}{c_p^*(T_{\mathrm{w}}^* - T_0^*)}, \quad \alpha = \frac{m^* n_{\mathrm{s}}^0}{\rho_0^*}.$$

Here, α is the mass-loading ratio of the particles and Ec the gas Eckert number. The first three dimensionless parameters above can be easily obtained using the Rankine–Hugoniot relations:

$$a = \frac{(\gamma+1)M^2}{2 + (\gamma-1)M^2},$$
$$d = \frac{(\gamma+1)^2 M^2}{[2 + (\gamma-1)M^2][2\gamma M^2 - (\gamma-1)]},$$
$$Ec = \frac{[2 + (\gamma-1)M^2]^2}{2(1+\gamma M^2)(1 - M^2)}.$$

For the dispersed phase, we introduce the Lagrangian coordinates (t, x_0), where $t = t^* U_0^*/l^*$ is the dimensionless time of the particle motion along the given trajectory from its trajectory origin on the wall and x_0 the abscissa of this origin. For a fixed trajectory, the dimensionless governing equations are given (here the subscript i is omitted):

$$\frac{\mathrm{d}x_{\mathrm{s}}}{\mathrm{d}t} = u_{\mathrm{s}},$$
$$\frac{\mathrm{d}\eta_{\mathrm{s}}}{\mathrm{d}t} = v_{\mathrm{s}},$$
$$\frac{\mathrm{d}u_{\mathrm{s}}}{\mathrm{d}t} = K\theta(u - u_{\mathrm{s}})D, \tag{8}$$
$$\frac{\mathrm{d}v_{\mathrm{s}}}{\mathrm{d}t} = K\theta(v - v_{\mathrm{s}})D - \kappa(u - u_{\mathrm{s}})H\left(K\theta\rho\left|\frac{\partial u}{\partial \eta}\right|\right)^{1/2} - \omega,$$
$$\frac{\mathrm{d}T_{\mathrm{s}}}{\mathrm{d}t} = \frac{2\chi}{3Pr}K\theta(T - T_{\mathrm{s}})G.$$

In Eq. (8), three dimensionless parameters are defined as:

$$\chi = \frac{c_p^*}{c_{\mathrm{s}}^*}, \quad \kappa = \frac{6.46}{12\pi\sqrt{6}}\left(\frac{2\rho_{\mathrm{s}}^0}{\rho_0^*}\right)^{1/4} Re_0^{3/2},$$
$$\omega = \frac{\mathrm{g}^* l^*}{U_0^{*2}}\left(\frac{\rho_{\mathrm{s}}^0}{18\rho_0^*}\right)^{1/2} Re_0,$$

where c_s^* is the specific heat of the particle material and $Re_0 = 2U_0^*\rho_0^*\sigma^*/\mu_0^*$ the particle Reynolds number. From the above mathematical formulation of the problem under consideration, it is not difficult to find the following nine independent similarity criteria for the dynamic behaviour of the near-wall two-phase flows induced by shock waves: $M, \gamma, Pr, K, \alpha, \chi, \kappa, \omega$ and Re_0. Sometimes, the Froude number $Fr = U_0^*/(g^*l^*)^{1/2}$ can be equivalently used instead of the criterion ω. Obviously, the latter five criteria appear because of the particle presence. When the parameter α is small ($\alpha \to 0$), the particle effect on the carrier-phase flow is negligible and only the first four similarity criteria determine the dynamic behaviour of the carrier phase, which is the same as in the pure-gas boundary layer case. However, in the small α case, the dispersed-phase flow is determined by all the other eight similarity criteria.

As mentioned before, the dust concentration is of concern in many practical applications and, following the novel method developed by Osiptsov et al. [21], the continuity equation of the dispersed phase in the Lagrangian variables is derived for the problem under consideration:

$$\frac{1}{n_s(t,x_0)} = |J|\,,$$
$$J = u_s\frac{\partial \eta_s(t,x_0)}{\partial x_0} - v_s\frac{\partial x_s(t,x_0)}{\partial x_0}. \tag{9}$$

Here $|J|$ is the modules of the Jacobian of the transformation from the Eulerian to Lagrangian variables. In the problem of the shock-induced near-wall two-phase flows, for the carrier phase, the boundary conditions are given on the shock front, on the wall and at the outer edge of the boundary layer:

$$\begin{aligned} &x = 0,\ \eta > 0\ :\ u = T = 1,\ v = 0;\\ &x \geq 0,\ \eta = 0\ :\ u = T = a,\ v = 0;\\ &x > 0,\ \eta \to \infty\ :\ u = 1,\ T = 1. \end{aligned} \tag{10}$$

For the dispersed phase, the initial conditions at $t = 0$ are given as

$$\begin{aligned} &x_s = x_0, \quad \eta_s = 0, \quad u_s = T_s = a, \quad v_s \to 0,\\ &n_s v_s = 1. \end{aligned} \tag{11}$$

Here returning particles are assumed to be redeposited on the wall and not rebound. In other words, all the ascending particles are aerodynamically entrained from the wall. The conditions (11) mean that the particles leave the wall at a vanishingly small velocity but the number flux of the particles (N^0) is a given finite quantity. In this work, the reference quantity for normalizing the particle number density is $n_s^0 = N^0/U_0^*$. It should be noted that, for simplicity, the upward particle flux at the surface is assumed to be constant. This boundary condition is not a crucial assumption and, in principle, the generalization from a constant value N^0 to any specified function $N^0(x)$ is straightforward. However, the boundary condition $v_s \to 0$ is a crucial one which allows our numerical modelling to possess the physical feature of the particle entrainment induced purely by the shear flow.

3 Solution method

In the small α case, we can first solve the governing equations (6) for the carrier phase and then the governing equations (8), (9) for the dispersed phase because the gas flow field does not change due to particle entrainment. In fact, as mentioned above, it is a real situation for the shock-induced dust cloud considered in this work. Besides, the laminar flow exists at the initial stage of the gas boundary layer in the neighbourhood region behind the shock front, where the effects of the particles in micron sizes are not yet manifested even at a finite value of the mass-loading ratio [22]. Hence the carrier-phase parameters can be calculated separately using the usual solution method for boundary-layer flows of a compressible gas. Moreover, according to the boundary layer theory [23], the gas temperature T^* depends only the gas tangential velocity u^* when $Pr = 1$ and it represents the solution for the carrier phase in its simplest form. When the wall temperature T_w^* keeps constant, the relation between T and u in the dimensionless variables can be derived as:

$$T = 1 + \left[\frac{Ec}{2}(1-a^2) - 1\right](1-u) + \frac{Ec}{2}(a-1)(1-u^2). \tag{12}$$

Following the usual procedure for finding the self-similar solution to the compressible-gas boundary layer equations [23], it is convenient to introduce the Illingworth–Stewartson transformation and similarity variables:

$$x_1 = Kx, \quad \eta_1 = \frac{1}{\sqrt{x_1}}\int_0^\eta \rho\,\mathrm{d}\eta, \quad \psi = f(\eta_1)\sqrt{x_1}, \tag{13}$$

where the dimensionless steam function ψ satisfies: $\partial\psi/\partial\eta = \rho u$ and $\partial\psi/\partial x = -\rho v$. The gas velocity and temperature in the boundary layer can be expressed in terms of $f(\eta_1)$ as follows:

$$
\begin{aligned}
u &= f'(\eta_1),\\
v &= -K\theta\left[\frac{f}{2\sqrt{x_1}} + \sqrt{x_1}f'\frac{\partial\eta_1}{\partial x_1}\right],\\
T &= 1 + \left[\frac{Ec}{2}(1-a^2)\right](1-f') + \frac{Ec}{2}(a-1)(1-f'^2).
\end{aligned}
\tag{14}
$$

Here the prime denotes differentiation with respect to η_1: $f' = \mathrm{d}f/\mathrm{d}\eta_1$. Then Eq. (6) reduces to a boundary-value problem for the Blasius function $f(\eta_1)$:

$$
2f''' + ff'' = 0, \tag{15}
$$

with boundary conditions:

$$
f(0) = 0\,, \quad f'(0) = a\,, \quad f'(\infty) = 1. \tag{16}
$$

The ordinary differential equation (15) can be easily solved numerically for a specified value of the shock Mach number.

For determining the dispersed-phase parameters (particularly, the number density of the particles n_s) on a fixed particle trajectory, values of the derivatives $\partial x_\mathrm{s}/\partial x_0$ and $\partial\eta_\mathrm{s}/\partial x_0$ in Eq. (9) should be known. The equations for these derivatives can be derived by differentiating the first four equations of the dispersed-phase equations (8) with respect to x_0:

$$
\begin{aligned}
\frac{\mathrm{d}w_1}{\mathrm{d}t} &= w_2,\\
\frac{\mathrm{d}w_3}{\mathrm{d}t} &= w_4,\\
\frac{\mathrm{d}w_2}{\mathrm{d}t} &= K\theta(u-u_\mathrm{s})\frac{\partial D}{\partial x_0} + K\theta(\frac{\partial u}{\partial x_0} - w_2)D\\
&\quad + K(u-u_\mathrm{s})D\frac{\partial\theta}{\partial x_0},\\
\frac{\mathrm{d}w_4}{\mathrm{d}t} &= K\theta(v-v_\mathrm{s})\frac{\partial D}{\partial x_0} + K\theta(\frac{\partial v}{\partial x_0} - w_4)D\\
&\quad + K(v-v_\mathrm{s})D\frac{\partial\theta}{\partial x_0}\\
&\quad - \kappa(u-u_\mathrm{s})\frac{\partial}{\partial x_0}\left[H\left(K\theta\rho\left|\frac{\partial u}{\partial\eta}\right|\right)^{1/2}\right]\\
&\quad - \kappa\left[H\left(K\theta\rho\left|\frac{\partial u}{\partial\eta}\right|\right)^{1/2}\right](\frac{\partial u}{\partial x_0} - w_2).
\end{aligned}
\tag{17}
$$

Here, $w_1 = \partial x_\mathrm{s}/\partial x_0, w_2 = \partial u_\mathrm{s}/\partial x_0, w_3 = \partial\eta_\mathrm{s}/\partial x_0$ and $w_4 = \partial v_\mathrm{s}/\partial x_0$. The initial conditions for Eq. (17) are as follows:

$$
t = 0 : w_1 = 1,\ w_2 = 0,\ w_3 = 0,\ w_4 = 0. \tag{18}
$$

For various x_0, the closed system of ordinary differential equations (8) and (17) can be numerically integrated on the given fixed trajectory and the algebraic relation (9) can be used to calculate n_s.

4 Computational results

The purpose of this study is to understand the main features of the shock-induced near-wall two-phase flow resulting from the local shear action. Thus the computations were performed for several values of the dynamic parameters (M, Re_0, κ and ω) but at fixed values of the thermodynamic properties ($Pr = K = \chi = 1, \gamma = 1.4$). In our calculations, the air is considered as the carrier phase. For reference, some typical values of relevant characteristic parameters are given in Table 1, in which the heavy particle ($\rho_\mathrm{s}^0 = 2.70\,\mathrm{g/cm^3}$) and the light particle ($\rho_\mathrm{s}^0 = 1.35\ \mathrm{g/cm^3}$) represent, respectively, metallic powders (i.e. aluminium) and organic powders (such as cornstarch and coal). In addition, within the framework of the model developed here, the assumption of laminarity of the gas boundary layer flow is valid in the neighbourhood of the shock front. On the basis of the boundary layer theory [23], in the flat plate case, transition from the laminar to the turbulent flow takes place at the critical Reynolds number which ranges over $Re_\mathrm{crit} = 3\times10^5$–$3\times10^6$ and the transfer of heat from the gas to the wall has a highly stabilizing effect on the subsonic boundary layer behind the shock wave. Then, based on the data in Table 1, the dimensionless abscissa x_crit of the point of transition can be determined from the known value of Re_crit. For example, in the $M = 2.0$ case, the transition position on the wall is estimated as $x_\mathrm{crit} \simeq 100, 1, 0.01$, respectively, for the aluminium particles of $1, 10, 100\,\mu\mathrm{m}$ diameter. However, we present numerical results for further downstream region as, in every turbulent flow, there exists a laminar sub-layer next to the wall where the shear lift force affects the particle rising from the bed surface to an important degree. Moreover, the transition involves a noticeable change in the velocity distribution curve. In other words, profiles of the gas tangential velocity become fuller owing to turbulence. This leads to a large increase in the flow shear action [23]. Therefore, our results are of significance for not only the laminar initial region but also the turbulent downstream. It is obvious that, for the turbulent region after the point of the transition, they provide a lower estimation of the aerodynamic entrainment capability of a moving shock wave.

In the $M = 2.0$ case, for the $10\,\mu\mathrm{m}$ aluminium particles ($\rho_\mathrm{s}^0 = 2.70\,\mathrm{g/cm^3}$), the velocity and temperature profiles of the two phases are plotted, respectively, in Figs. 1, 2 and 3, where the longitudinal coordinates for six different positions behind the shock front take the values as $x = 0.5, 1, 2, 4, 6, 10$, respectively. It is seen that, in the similarity coordinate $\eta/\sqrt{x}$, the dispersed-phase flow is not self-similar like the carrier-phase flow. Clearly, the particles are not in equilibrium with the

Table 1 Typical values of characteristic parameters

M	ρ_s^0(g/cm^3)	$2\sigma^*$(μm)	l^*(cm)	Re	Re_0	κ	ω
2.0	2.70	1	1.434×10^{-1}	4.246×10^4	2.961×10^1	7.287×10^1	4.273×10^{-5}
2.0	2.70	10	1.434×10^1	4.246×10^6	2.961×10^2	2.304×10^3	4.273×10^{-2}
2.0	2.70	100	1.434×10^3	4.246×10^8	2.961×10^3	7.287×10^4	4.273×10^1
2.0	1.35	10	7.170×10^0	2.123×10^6	2.961×10^2	1.938×10^3	1.511×10^{-2}
1.5	2.70	10	1.837×10^1	4.864×10^6	2.648×10^2	2.133×10^3	5.080×10^{-2}

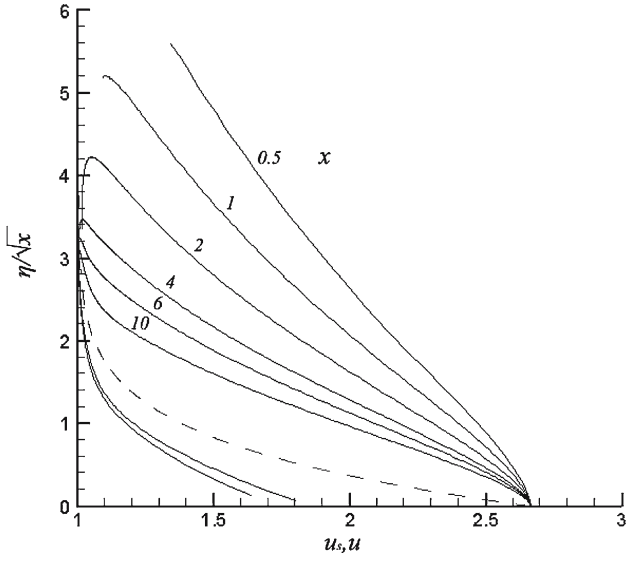

Fig. 1 The tangential velocity profiles for the two phases at $M = 2.0$, $Re_0 = 300$, $\kappa = 2,300$ and $\omega = 0.04$. The *broken line* is for the carrier phase and *solid line* for the dispersed phase

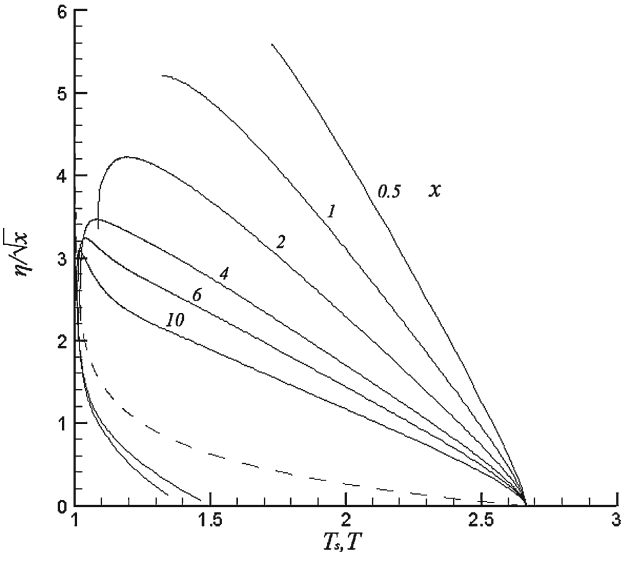

Fig. 3 The temperature profiles for the two phases at $M = 2.0$, $Re_0 = 300$, $\kappa = 2,300$ and $\omega = 0.04$. The *broken line* is for the carrier phase and *solid line* for the dispersed phase

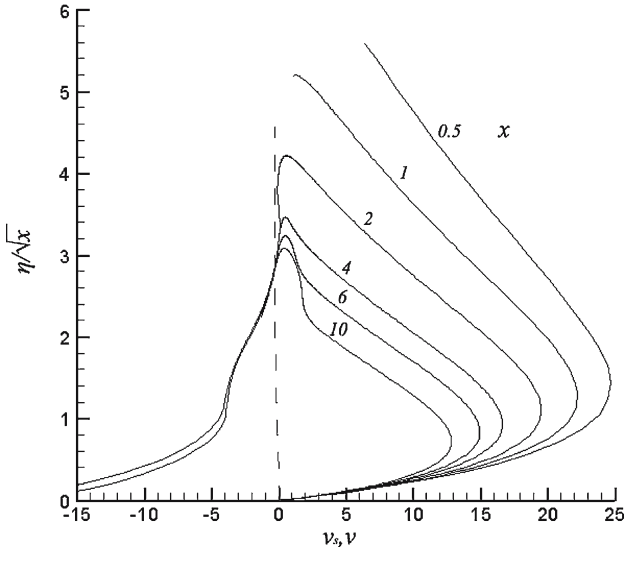

Fig. 2 The normal velocity profiles for the two phases at $M = 2.0$, $Re_0 = 300$, $\kappa = 2,300$ and $\omega = 0.04$. The *broken line* is for the carrier phase and *solid line* for the dispersed phase

carrier phase in the gas boundary layer and there exist apparent velocity and temperature differences between the two phases inside the dust cloud. Especially, owing to the lift force, the normal velocity of the dispersed phase is very large compared with that of the carrier phase (see Fig. 2). With increasing distance from the shock front, the velocity slip and temperature jump between the two phases decrease because the local flow shear decreases. It is also found from Figs. 1, 2 and 3 that, at the given control parameters ($M = 2.0$, $Re_0 \simeq 300$, $\kappa \simeq 2,300$ and $\omega \simeq 0.04$), the particles can be entrained out of the gas boundary layer and into the outer flow. As mentioned above, the aerodynamic entrainment capability of a moving shock wave becomes weaker with increase in the distance from its front and, at some downstream position (say, $x \simeq 2$ in the case under consideration), the entrained particles make their motion only in the gas boundary layer. The envelope of the trajectory family of the entrained particles consists of the outer boundary of the shock-induced dust cloud. In general, the dust-cloud boundary does not coincide with the outer edge of the

gas boundary layer and, in the neighbourhood of the shock front, the former is higher than the latter for large values of the similarity parameter κ (say, $\kappa = 2,300$).

For the same shock Mach number but 1 μm aluminium particles, the obtained flow structure is given in Figs. 4, 5 and 6, where the longitudinal coordinates for six different profiles take the values as $x = 50$, 100, 200, 400, 600, 1,000, respectively. In this way, the corresponding profiles for the 1 and 10 μm aluminium particles are located at the same dimensional position in the laboratory reference framework (cf. Table 1). It is found that, under the action of the same shear lift, the 1 μm particles cannot be entrained out of the gas boundary layer. In other words, the rising height of the entrained particles depends on not only the flow shear of the gas boundary layer but also the size or material density of the particles. The similarity parameter κ represents the effect of physical properties of the particles on their entrainment behaviour. Our calculations for the front-neighbourhood region (although they are not shown here) indicate that, at the given control parameters ($M = 2.0$, $Re_0 \simeq 30$, $\kappa \simeq 70$ and $\omega \simeq 0$), the dust cloud is enclosed totally inside the gas boundary layer. This phenomenon is not difficult to understand as, at a small value of κ (say, $\kappa = 70$), the normal velocities of the 1 μm particles decrease by more than one order in magnitude compared with those of the 10 μm particles (see Figs. 2 and 5). Besides, these results show that, as the particle size decreases, the interphase differences in the tangential velocity and temperature decrease too.

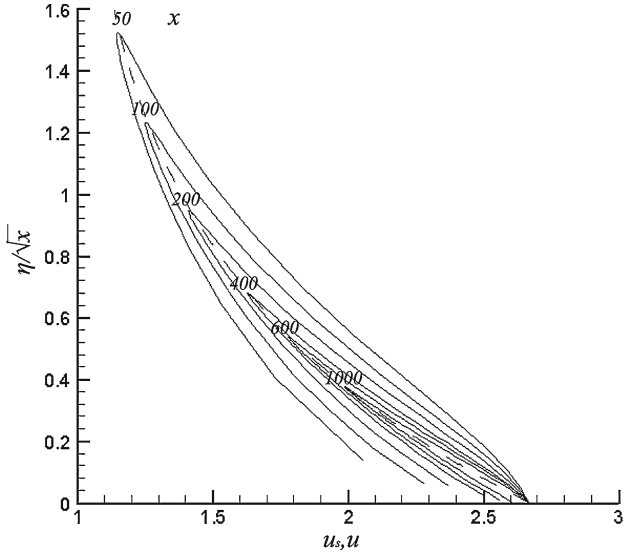

Fig. 4 The tangential velocity profiles for the two phases at $M = 2.0$, $Re_0 = 30$, $\kappa = 70$ and $\omega = 0$. The *broken line* is for the carrier phase and *solid line* for the dispersed phase

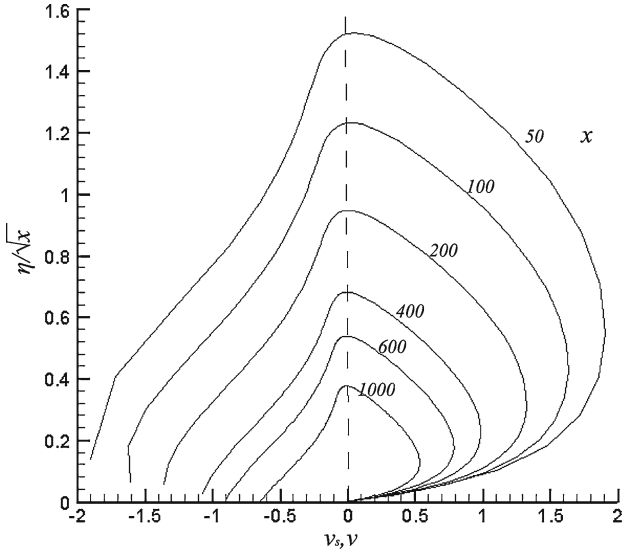

Fig. 5 The normal velocity profiles of the two phases at $M = 2.0$, $Re_0 = 30$, $\kappa = 70$ and $\omega = 0$. The *broken line* is for the carrier phase and *solid line* for the dispersed phase

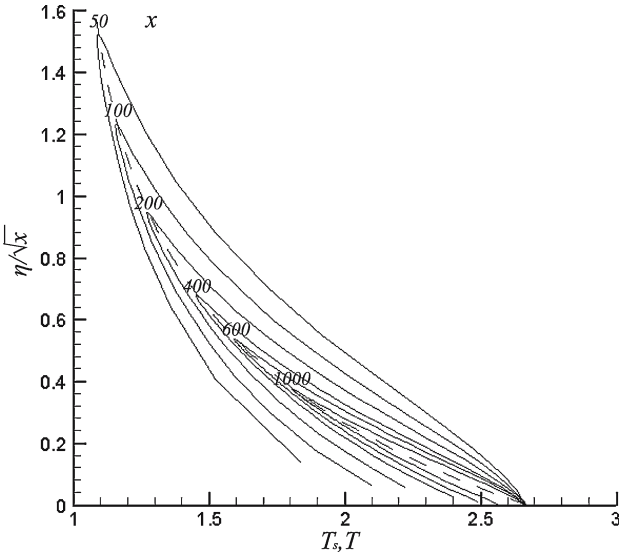

Fig. 6 The temperature profiles of the two phases at $M = 2.0$, $Re_0 = 30$, $\kappa = 70$ and $\omega = 0$. The *broken line* is for the carrier phase and *solid line* for the dispersed phase

From Figs. 1, 2, 3, 4, 5 and 6, it is interesting to note that the particle parameters possess two-valued feature because two particle trajectories intersect each other inside the dust cloud. Specifically, the particles having two-valued parameters correspond to those curves where a vertex, a right branch and a left branch exist. These two branches are divided at the vertex and developed, respectively, on the right and left sides of each curve. It is found in Figs. 2 and 5 that, for these particle parameters curves, the right branches always represent the ascending particles with positive normal velocity while the left branches may correspond to the

descending particles with negative normal velocity or to the ascending particles as well. As usual, the terms "ascending" and "descending" refer to $v_s > 0$ and $v_s < 0$, respectively. In general, it is easy to imagine that the trajectory intersection takes place between the ascending and descending parts. However, this phenomenon reveals that, in a narrow zone near the outer boundary of the dust cloud, particle trajectories may intersect on their ascending parts at a large value of κ (say, $\kappa > 2,000$). Finally, the obtained results shown in these figures indicate that, with respect to the longitudinal coordinate x, the profiles of the particle velocity and temperature develop in a similar way and then we discuss only the development of the particle tangential velocity below.

For three different groups of the control parameters, the profile development of the particle tangential velocity is shown, respectively in Fig. 7 ($M = 2.0$, $Re_0 \simeq 3,000$, $\kappa \simeq 70,000$ and $\omega \simeq 40$), Fig. 8 ($M = 2.0$, $Re_0 \simeq 300$, $\kappa \simeq 1,940$ and $\omega \simeq 0.01$) and Fig. 9 ($M = 1.5$, $Re_0 \simeq 265$, $\kappa \simeq 2,100$ and $\omega \simeq 0.05$). Here, the first group corresponds to the flow of the 100 μm aluminium particles at $M = 2.0$, the second one to that of the 10 μm cornstarch (or coal) particles at $M = 2.0$ and the third one to that of the 10 μm aluminium particles at $M = 1.5$. Similarly, the six profiles for the 100 μm aluminium particles (see Fig. 7) are located in the same dimensional positions as those for the 10 and 1 μm aluminium particles (see Figs. 1, 4). Due to the extremely large value of κ, the 100 μm aluminium particles are entrained far out of the gas boundary layer although

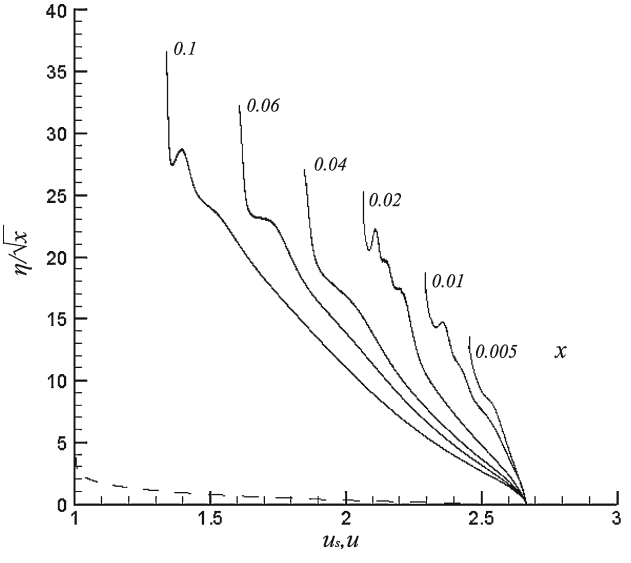

Fig. 7 Development of the particle tangential velocity profiles at $M = 2.0$, $Re_0 = 3,000$, $\kappa = 7,0000$ and $\omega = 40$. The *broken line* is for the carrier phase and *solid line* for the dispersed phase

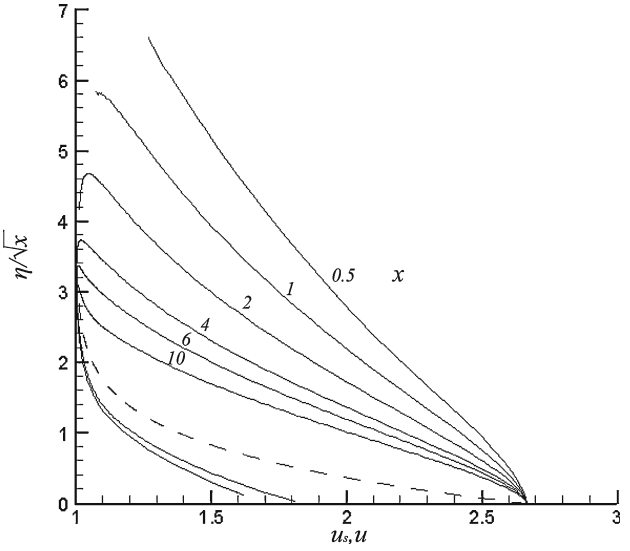

Fig. 8 Development of the particle tangential velocity profiles at $M = 2.0$, $Re_0 = 300$, $\kappa = 1,940$ and $\omega = 0.01$. The *broken line* is for the carrier phase and *solid line* for the dispersed phase.

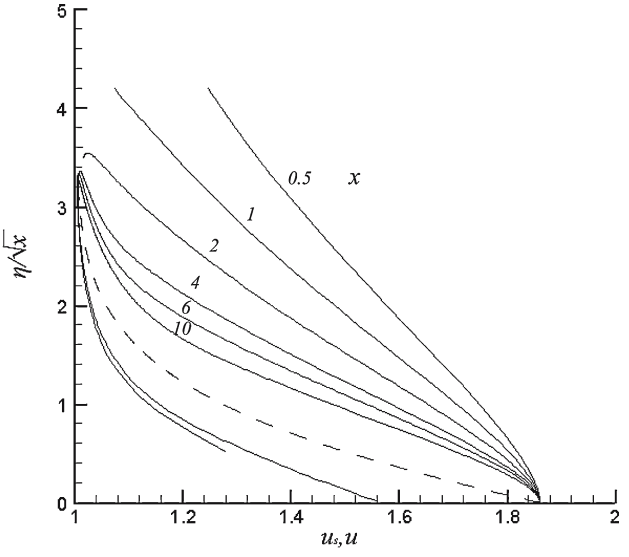

Fig. 9 Development of the particle tangential velocity profiles at $M = 1.5$, $Re_0 = 265$, $\kappa = 2,100$ and $\omega = 0.05$. The *broken line* is for the carrier phase and *solid line* for the dispersed phase

the local flow shear is the same for the three different sized particles. It is more interesting that, inside the dust cloud of the 100 μm aluminium particles, there are some points at which three particle trajectories intersect (see curves at $x = 0.01, 0.02$ and 0.1 in Fig. 7). Comparison between the results for different material densities ($\rho_s^0 = 1.35$ or $2.70\,\mathrm{g/cm^3}$) but at the same shock Mach number ($M = 2.0$) in Figs. 8 and 1 indicates that the intersection of the particle trajectories occurs almost at the same dimensionless position ($x \simeq 1$) for both the cornstarch (or coal) and aluminium particles when they

have the same diameter ($2\sigma^* = 10\,\mu$m). Clearly, it is because that, in these two cases, the control parameters M, Re_0 take the same values and the values of the parameter κ are very close. However, due to the decrease in the parameter ω, the dust cloud of the cornstarch particles becomes much higher than that of the aluminium particles in the dimensionless variables. On the other hand, the effect of the shock Mach number on the particle motion can be shown by comparing the results in Fig. 9 for $M = 1.5$ and in Fig. 1 for $M = 2.0$. For the $10\,\mu$m aluminium particles, the phenomenon of the trajectory intersection in the case $M = 1.5$ happens at a further downstream position $x \geq 2$. In addition, in the proximity of the shock front, the dimensionless height of the dust cloud decreases significantly when the shock Mach number changes from 2.0 to 1.5. Obviously, the decrease in the shock Mach number leads to the decrease in the local flow shear, which in turn changes the behaviour of the particle motion. Of course, the obtained results show that, in a wide range of the control parameters and the longitudinal coordinates, interphase non-equilibrium is a common feature of the near-wall two-phase flows induced by a shock wave moving over a particles bed. In addition, taking the lift force into account results in the intersection of the particle trajectories and the non-uniqueness in the flow parameters of the dispersed phase inside the dust cloud.

For the case of the 10 and $1\,\mu$m aluminium particles at $M = 2.0$, the particle number density profiles at six different positions are shown in Figs. 10 and 11, where the stretched coordinate η is used instead of the similarity coordinate $\eta/\sqrt{x}$. As mentioned before, at each

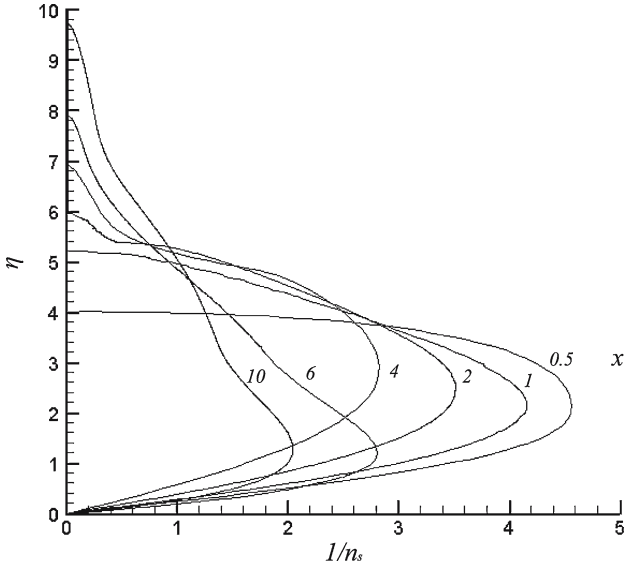

Fig. 10 Development of the particle number density profiles at $M = 2.0$, $Re_0 = 300$, $\kappa = 2,300$ and $\omega = 0.04$

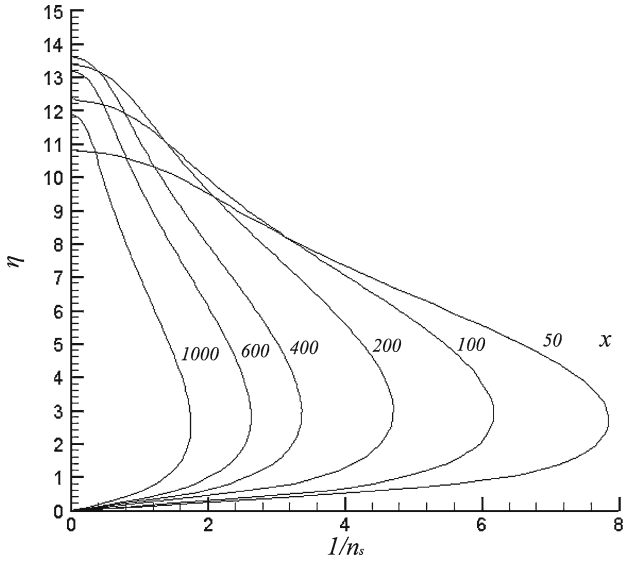

Fig. 11 Development of the particle number density profiles at $M = 2.0$, $Re_0 = 30$, $\kappa = 70$ and $\omega = 0$

point in the zone of intersecting particle trajectories, two or three trajectories intersect and integration of Eqs. (8), (9) and (17) gives the number density of one particle continuum along a fixed trajectory only. Therefore, to calculate the number density distribution inside the dust cloud, it needs to sum up the number densities of the particle continua along all the ascending and descending trajectories crossing the specified point of space. From the development of the particle number-density profiles shown in Figs. 10 and 11, it is seen that, in proximity of the shock front, the height of the dust cloud increases with increasing x (see Fig. 10) but, in far downstream region, this height may decrease with increasing x (see curves at $x = 400, 600, 1,000$ in Fig. 11). This is because in far downstream region, the local flow shear action weakens as the gas boundary layer thickens. Besides, the results in Figs. 10 and 11 indicate that, along each profile, the maximum density of the dispersed phase is reached on the erodible surface and on the outer boundary of the dust cloud. The first maximum value appears due to the vanishingly small normal velocity but finite number flux on the surface of the particles bed [see the conditions (11)]. The second maximum value appears due to the zero modules of the Jacobian on the outer boundary of the dust cloud. As a result, the number density of the dispersed phase n_s grows unbounded. However, this type of singularity is integrable and then the dilute model is valid for the range of the control parameters considered in this work [24]. The phenomenon of sharp stratification of the dispersed phase and formation of local particle accumulation zone near the envelope of the particle trajectory family is

of significance in estimating the explosibility limits of gas–particle mixtures.

5 Conclusion

The numerical modelling of the flows induced by a normal shock wave travelling, at a constant speed, over a micron-sized particles bed is developed. In the shock-fixed coordinates, the governing equations and similarity criteria are given for the near-wall two-phase flows. For the small mass-loading ratio case, computations are performed in a wide range of the control parameters (M, Re_0, κ and ω) and they provide an estimation of the aerodynamic entrainment capability of the gas boundary layer behind the shock wave. The particles are raised into the air under the action of the lift force resulting from the local flow shear, which depends on the shock Mach number M and the distance from the shock front x. Taking the shear lift force into account leads to intersection of the particle trajectories and non-uniqueness in the flow parameters of the dispersed phase. For the same shear action, behaviour of the particle motion is influenced mainly by the similarity parameter κ. At large values of κ, the particles can be entrained out of the gas boundary layer and two or three trajectories may intersect on the ascending part of their trajectories in the narrow zone near the outer boundary of the dust cloud. The full Lagrangian method adopted can overcome the difficulty in calculating the particle flow field with the multiple-valued-point zone. The obtained results indicate that interphase non-equilibrium in the velocity and temperature is the common feature of the shock-induced near-wall two-phase flows over the particles bed. Concerning the number density of the dispersed phase, a local particle accumulation zone forms near the envelope of the particle trajectory family.

Acknowledgements This work received financial support from the Natural Science Foundation of China (NSFC grant No. 90205024).

References

1. Bielert, U., Sichel, M.: Numerical simulation of dust explosions in pneumatic conveyors. Shock Waves **2**, 125–139 (1999)
2. Zhang, F., Grönig H., van de Ven A.: DDT and detonation waves in dust–air mixtures. Shock Waves **11**, 53–71 (2001)
3. Khasainov, B.A., Veyssiere, B.: Initiation of detonation regimes in hybrid two-phase mixtures. Shock Waves **6**, 9–15 (1996)
4. Veyssiere, B., Khasainov, B.A., Arfi, P.: Investigation of the detonation regimes in gaseous mixtures with suspended starch particles. Shock Waves **9**, 165–172 (1999)
5. Tsuboi, N., Hayashi, A.K., Matsumoto, Y.: Three-dimensional parallel simulation of cornstarch-oxygen two-phase detonation. Shock Waves **10**, 277–285 (2000)
6. Veyssiere, B., Ingignoli, W.: Existence of the detonation cellular structure in two-phase hybrid mixtures. Shock Waves **12**, 291–299 (2003)
7. Carvel, R.O., Thomas, G.O., Brown, C.J.: Some observations of detonation propagation through a gas containing dust particles in suspension. Shock Waves **13**, 83–89 (2003)
8. Benkiewicz, K., Hayashi, K.: Two-dimensional numerical simulations of multi-head detonation in oxygen-aluminum mixtures using an adaptive mesh refinement. Shock Waves **12**, 385–402 (2003)
9. Merzkirch, W., Bracht, K.: The erosion of dust by a shock wave in air: initial stage with laminar flow. Int. J. Multiph Flow **4**, 89–95 (1978)
10. Hwang, C.C.: Initial stage of the interaction of a shock wave with a dust deposit. Int. J. Multiph. Flow **12**, 655–666 (1986)
11. Outa, I., Tajima, K., Kabayashi, M., Miura, S.: Boundary layer of non-equilibrium gas–particle mixture modified by particle lifting motion behind a shock front. In: Proceedings of 17th International Symposium on Shock Waves and Shock Tubes, Bethlehem, USA, pp. 770–775 (1989)
12. Wu, Q., Wang, B.Y.: Numerical analysis of dust particle entrainment induced by shock waves. In: Zhang Guanren, Z. (ed.) Proceedings of the Second International Symposium on Intense Dynamic Loading and Its Effects. Sichuan University Press, Chengdu pp. 167–170 (1992)
13. Thevand, N., Daniel, E.: Numerical study of the lift force influence on two-phase shock tube boundary layer characteristics. Shock Waves **11**, 279–288 (2002)
14. Crowe, C.T.: Review—numerical modeles for dilute gas-particle flow. ASME J. Fluid Eng. **104**, 297–303 (1982)
15. DiGiacinto, M., Sabetta, F., Piva, R.: Two-way coupling effects in dilute gas-particle flows. ASME J. Fluid Eng. **104**, 304–312 (1982)
16. Marble, F.E.: Dynamics of dusty gases. Annu. Rev. Fluid Mech. **2**, 397–446 (1970)
17. Carlson, D.J.: Hoglund, R.F.: Particle drag and heat transfer in rocket nozzles. AIAA J. **2**, 1980–1984 (1964)
18. Fuchs, N.A.: Mechanics of Aerosols. MacMillan, New York (1964)
19. Saffman, P.G.: The lift on a small sphere in a slow shear flow. J. Fluid Mech. **22**, 384–400 (1965); Corrigendum. J. Fluid Mech. **31**, 624 (1968)
20. Mei, R.: An approximate expression for the shear lift force on a spherical particle at finite Reynolds number. Int. J. Multiph. Flow **18**, 145–147 (1992)
21. Osiptsov, A.N., Rozin, A.V., Teverovskii, M.A., Wang, B.Y.: Novel Lagrangian method for calculating the particle concentration in dusty-gas flows with intersecting particle trajectories. In: Lixing, Z., Xiangfan, L. (eds.) Proceedings of International Symposium on Multiphase Fluid, Non-Newtonian Fluid and Physico-Chemical Fluid Flows. Academic Publishers, Beijing, pp. 2-65–2-72 (1997)
22. Wang, B.Y., Glass, I.I.: Boundary layer flows behind constant speed shock waves moing into a dusty gas. Shock Waves **1**, 135–144 (1991)
23. Schlichting, H.: Boundary Layer Theory, 7th edn. McGraw-Hill, New York (1979)
24. Osiptsov, A.N.: Investigation of zones of unbounded growth of particle concentration in dispese flows (in Russian). Izv. Akad. Nauk SSSR Mekh. Zhidk. Gaza **19**, 46–53 (1984)